Available online at www.sciencedirect.com
SCIENCE DIRECT®
Physica A 351 (2005) 142–158
PHYSICA A
www.elsevier.com/locate/physa

Randomness in the bouncing ball dynamics

S. Giusepponi[a], F. Marchesoni[a,*], M. Borromeo[b]

[a]*Dipartimento di Fisica, Università di Camerino, I-62032 Camerino, Italy*
[b]*Dipartimento di Fisica, and Istituto Nazionale di Fisica Nucleare, Università di Perugia, I-06123 Perugia, Italy*

Received 16 October 2004

Abstract

The dynamics of a vibrated bouncing ball is studied numerically in the reduced impact representation, where the velocity of the bouncing ball is sampled at each impact with the plate (asynchronous sampling). Its random nature is thus fully revealed: (i) the chattering mechanism, through which the ball gets locked on the plate, is accomplished within a limited interval of the plate oscillation phase, and (ii) is well described in impact representation by a special structure of looped, nested bands and (iii) chattering trajectories and strange attractors may coexist for appropriate ranges of the parameter values. Structure and substructure of the chattering bands are well explained in terms of a simple impact map rule. These results are of potential application to the analysis of high-temperature vibrated granular gases.

PACS: 46.70.Lk; 05.45.−a; 81.07.−b

1. Introduction

A problem as simple as the dynamics of a *Bouncing Ball* (BB) on an oscillating plate [1–4] keeps intriguing physicists despite the rich literature on or related to the subject [5–14]. This is, for example, the case of the archetypal model of an inelastic BB with constant restitution coefficient α (α is the ratio of the relative ball-plate velocity immediately after and before impact). While there is a general consensus on

*Corresponding author. Tel.: +39 329 260 9961; fax: +39 075 44666.
E-mail address: fabio.marchesoni@pg.infn.it (F. Marchesoni).

0378-4371/$ - see front matter
doi:10.1016/j.physa.2004.12.016

the irregular nature of the BB motion, the authors of Refs. [1,2] noticed that after a sufficiently large, possibly infinite number of bounces, the BB gets eventually locked onto the plate for a certain interval of one final oscillation cycle (*chattering mechanism*) and then relaunched at an appropriate oscillation phase. This implies that the dynamics of a vibrated inelastic BB would be ultimately *periodic*, at variance with: (a) Earlier theoretical studies [6–9], mostly based on the so-called high-bounce approximation (i.e., neglecting the amplitude of the plate oscillations versus the ball jump height) and focused on the evidence of period-doubling route to chaos; (b) Experimental observations on real BBs [14], where some manifestations of chaos seem, indeed, to emerge. It should be noticed that the validity of the ideal BB model in most experimental realizations is questionable. In real experiments, the restitution coefficient α depends on the ball impact velocity relative to the platform [12,15] and approaches unity for vanishingly small bounce amplitudes, i.e., right during the chattering process we are to investigate.

Chattering does not exclude the persistence of regular trajectories where a given sequence of q bounces repeats itself after an integer number k of plate oscillations. In principle, q (and k) may be extremely large, thus resulting in a truly chaotic trajectory even for $\alpha < 1$. Moreover, Tufillaro [3,4] showed numerically that for certain values of the model parameters, there exists an appreciable fraction of non-periodic BB orbits that may converge toward one (or more) strange attractors.

As a further motivation that inspired this work, we mention the extensive literature that focused recently on the physics of granular matter, in general, and on the dynamics of vibrated granular gases, in particular [11–14]. A granular gas can be regarded as an assembly of identical BB, each colliding inelastically with the walls of the container and the surrounding balls. Therefore, one expects that some of the results presented here may apply to the study of high-temperature (or low-density) vibrated granular gases as well [16].

In this paper we present a quantitative description of the chattering dynamics of an ideal inelastic ball bouncing on a vibrating platform. Our results are arranged as follows. In Section 2 we introduce the ideal BB model and show how its dynamics can be conveniently described in the reduced impact representation. In this representation the velocity of the bouncing ball is sampled at each impact with the plate. Moreover, we show how to reduce our analysis to a special region in the impact parameter space where all the BB trajectories get eventually trapped, with no exceptions (*trapping region*). In Section 3 we propose a simple impact map rule to determine the nth forward image of the trapping region. After n iterations the representative points of the trapping region are mapped into a characteristic *band structure* that for $\alpha < 1$ comprises a fixed number of extended bands and a countable set of $n-1$ looped, nested *chattering bands*; the latter ones insist upon a limited domain of the impact phase (*chattering phase*). In Section 4 we analyze the stability of the BB periodic trajectories, thus obtaining a condition for the existence of strange attractors—necessarily inside the trapping region. In most cases, one expects to detect just one attractor inside the top extended band of the first iterate of the trapping region; all attractors may be generated from a corresponding stable periodic orbit through period doubling. Our analysis of the BB chattering is not affected by the presence of strange attractors. In Section 5 we discuss the possibility of applying our results to the statistical analysis of high-temperature vibrated granular gases.

2. The ideal bouncing ball

The modelling of an ideal BB is really simple: A point-like unit mass with coordinate z_b impinges vertically on a rigid plate of infinite mass oscillating up and down with law $z_p(t) = -A\sin(\Omega t)$ (arbitrary time origin); the BB is subject to a uniform acceleration of gravity $-g$ and the inelastic nature of its instantaneous collisions with the plate is fully described by a constant restitution coefficient α. Here $\alpha \equiv (\dot{z}_b - \dot{z}_p)_+ / |\dot{z}_b - \dot{z}_p|_-$, where the subscripts denote the time instant, respectively, after $(+)$ and before $(-)$ the ball-plate impact (Fig. 1). All other forces (internal and external, alike) are neglected for simplicity. Dimensionless units are adopted throughout by expressing t in units of $T = 2\pi/\Omega$, and the vertical displacements $z_{b,p}$ in units of $gT^2/2$.

A closely related version of the BB problem is represented by the so-called *impact oscillator*, where an elastic restoring force attracts the ball toward the plate [10,17].

2.1. Impact representation

A BB trajectory can be mapped into a point process of impact events (Fig. 1a). The nth impact event is characterized by two dimensionless coordinates, the impact time τ_n and the relative velocity $W_n \equiv W(\tau_n)$ immediately after the impact (Fig. 1b), $W_n = \dot{z}_b(\tau_n+) - \dot{z}_p(\tau_n+) \geqslant 0$. As the trajectory between two consecutive impacts is known analytically, the relevant impact parameters are related through the implicit map

$$\frac{\Gamma}{2\pi}[\sin(2\pi\tau_{n+1}) - \sin(2\pi\tau_n)] + [W_n - \Gamma\cos(2\pi\tau_n)] \times (\tau_{n+1} - \tau_n) - (\tau_{n+1} - \tau_n)^2 = 0\,, \tag{1}$$

$$W_{n+1} = -\alpha W_n + 2\alpha(\tau_{n+1} - \tau_n) - \alpha\Gamma[\cos(2\pi\tau_{n+1}) - \cos(2\pi\tau_n)]\,. \tag{2}$$

The ideal BB dynamics is thus controlled by two parameters, only, the restitution coefficient α and the reduced acceleration $\Gamma \equiv A\Omega^2/\pi g$.

Starting with arbitrary initial conditions for bounce n, the impact map (1)–(2) may be iterated numerically forward and backward to determine the unique impact parameters of bounces $n+1$ and $n-1$, respectively; the iteration procedure can be repeated as many times as our computer accuracy allows. To avoid stretching the results out over several plate cycles the time axis can be folded as $\tau \to \bar{\tau} \equiv \tau \bmod[1]$. The ensuing reduced *impact representation* of the BB dynamics [1–4,9] has the topology of the half-cylinder $(0 \leqslant \bar{\tau} \leqslant 1, W \geqslant 0)$ drawn in Fig. 1c—see also Figs. 2 and 3.

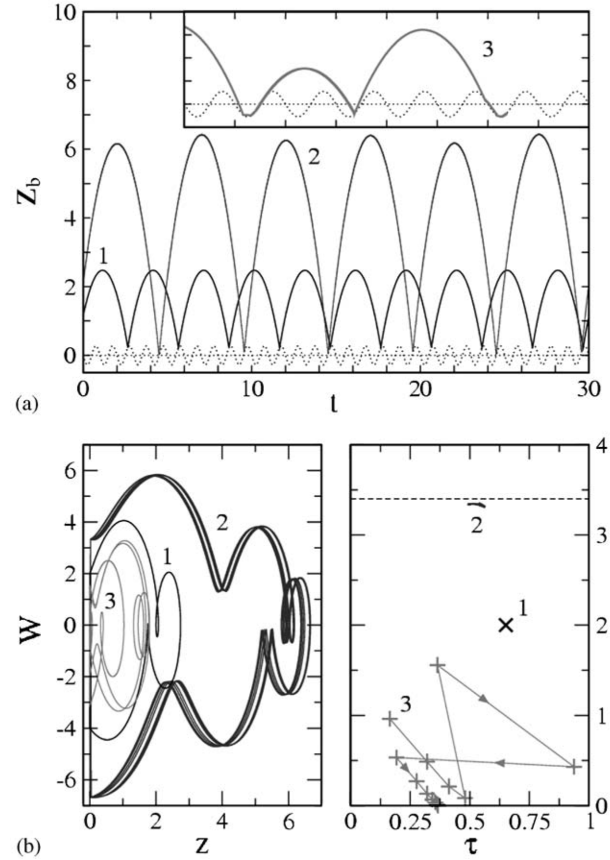

Fig. 1. Bouncing trajectories for $\alpha = 0.5$, $\Gamma = 1.724$ and $W_0 < \overline{W}_0 = 3.40$ and their representations: (a) Real-time representation, z_b vs. t, of three typical trajectories, (1) periodic, (2) chaotic and (3) chattering. The period of the plate oscillations $z_p(t)$ (dotted curve) sets the time scale; (b) Orbit of the trajectories of panel (a) in the (W, z) plane (relative ball-plate coordinates). Note that the stroboscopic representation (Section 5) is obtained by sampling this type of BB trajectories at regular time intervals nT; (c) reduced impact representation of the trajectories of panel (a): (1) one cross ($\times$); (2) dots; and (3) pluses ($+$). As in (a) we chose $W_0 < \overline{W}_0$ (dashed line), it follows immediately that here all representative points belong to the trapping region D^0.

The impact representation is based on an asynchronous sampling of the BB trajectories; the value of τ_n, the impact time of the nth bounce, varies greatly depending on the trajectory initial conditions. In particular, a chattering trajectory (Sections 2.2 and 3.2) can execute infinitely many bounces in less than one plate oscillation period T, while the bounces of the periodic trajectories may span over many a period T. The simplest synchronous representation of the BB dynamics utilizes the plate oscillations as an external clock, namely, all trajectories get sampled at the same time instant $\tau_n = nT + \tau_0$, where $n = 1, 2, \ldots,$ $\tau_0 = 0$ for convenience.

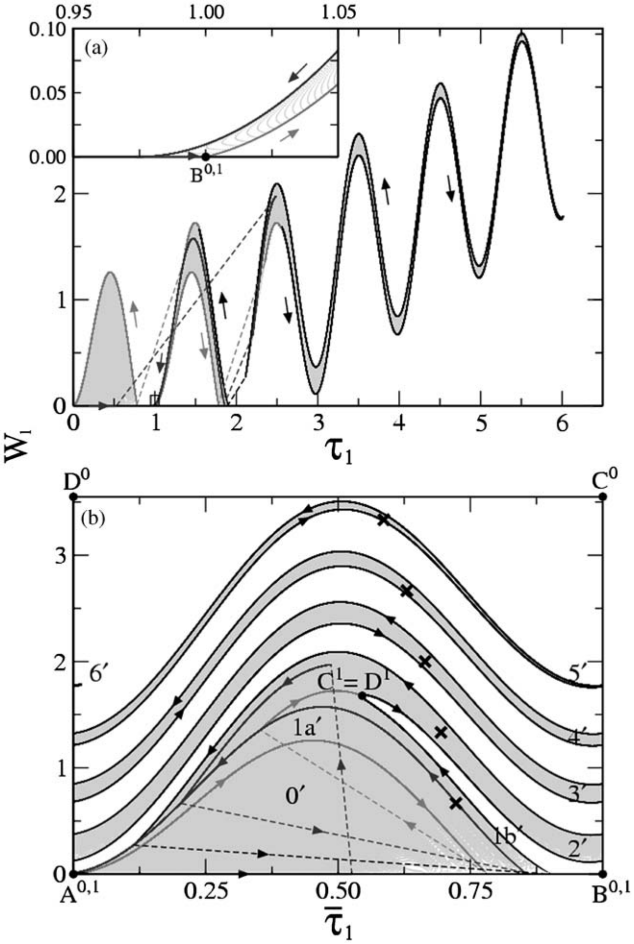

Fig. 2. Forward image of D^0 in extended (a) and reduced (b) impact representation for the generic case $\alpha = 0.5$, $\Gamma = 1.947$. The numerical estimates $\overline{W}_0 = 3.55$ and $\tau_{max} = 6.05$ compare well with $\overline{W}_0 = 4.10$, Eq. (3), and $\tau_{max} = 6.60$, Eq. (4). Accordingly, in panel (a) D^1 encroaches upon the seventh plate oscillation, while on folding, it develops six extended bands. The points belonging to band k' represent the impact parameters of the trajectories that bounce on the plate for the first time during the $(k+1)$th plate oscillation; the central region is labelled $0'$ as it represents the trajectories that bounce on the plate with $0 < \tau_1 \leqslant 1$. Both panels are limited from above by the boundary line $W_0 = \overline{W}_0$. The broken forward image of the counterclockwise oriented boundary lines $(AB)^0$, $(BC)^0$ and $(CD)^0$ are drawn in dark gray, light gray and black, respectively. In both panels, the non-uniformly shaded area represents the forward image of the uniform grid $(m/N_\tau, n\overline{W}_0/N_W)$, with $m = 0, 1, \ldots N_\tau$, $n = 0, 1, \ldots N_W$, and $N_\tau = 10^3$, $N_W = 720$, introduced to sample D^0. The inset of panel (a) is a blow up of the rectangle centered at $\tau_1 = 1$; the non-uniform distribution of the D^1 grid is apparent. The crosses ($\times$) denote the five stable periodic orbits allowed by our choice of the BB parameters (see Section 4).

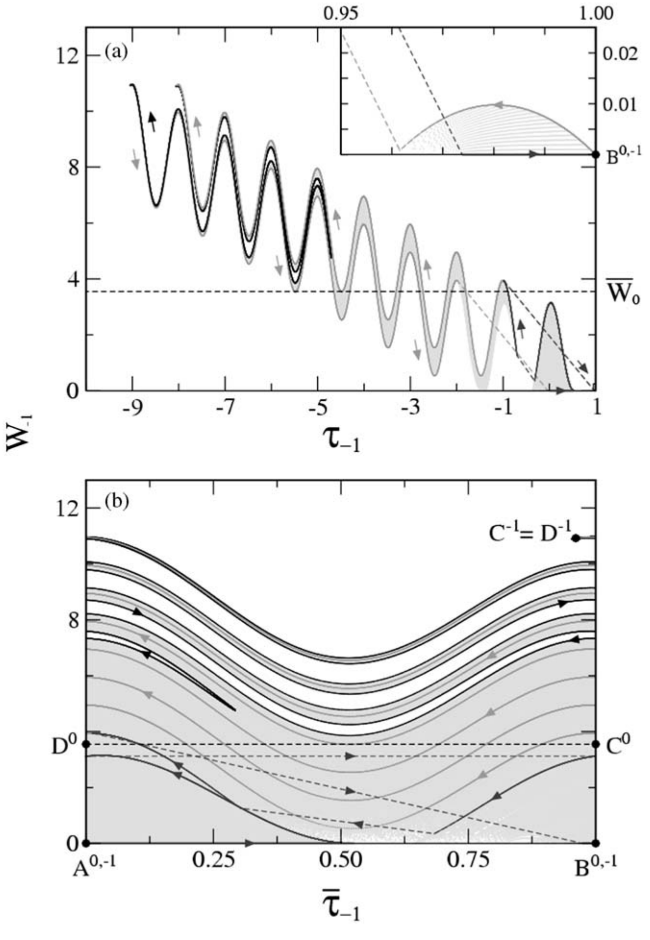

Fig. 3. Backward image of D^0 in extended (a) and reduced (b) impact representation for $\alpha = 0.5$, $\Gamma = 1.947$. In both panels the boundary line $W_0 = \overline{W}_0$ and the backward image of the uniform grid sampling D^0, see Fig. 2, are reported for reader's convenience. The broken backward image of the counterclockwise-oriented boundary lines $(AB)^0$, $(BC)^0$ and $(CD)^0$, panel (b), are drawn in dark gray, light gray and black, respectively. The band structure of D^{-1} in (b) results from the folding of the complicated extended pre-image of D^0 in (a).

This is the *stroboscopic* representation of the BB dynamics briefly mentioned in Section 5.

2.2. General features

We summarize now a few well-known properties [1–4] of the BB dynamics:

(i) *Launching mechanism*: The ball, placed on the moving plate, i.e., with $W_0 = 0$, sits on it until the plate acceleration overcomes the acceleration of gravity (i.e., $\Gamma \geqslant 1/\pi$). It follows that the locked state is stable for $0 \leqslant \tau_0 \leqslant \tau_g$ and $1 - \tau_f \leqslant \tau_0 \leqslant 1$, with $\tau_f = \tau_g - 1/2 = (1/2\pi)\arcsin(1/\pi\Gamma)$, and unstable for $\tau_g \leqslant \tau_0 \leqslant 1 - \tau_f$; therefore, the ball is launched by the plate with $\tau_0 = \tau_g$;

(ii) *Trapping region*: Its existence follows the observation that, no matter what τ_0, the impact velocity of the first jump W_1 is smaller than the initial impact velocity W_0 for all W_0 above a certain limiting value $\overline{W}_0$. This implies that all trajectories originated outside the trapping region $D(\overline{\tau}, W) \equiv (0 \leqslant W \leqslant \overline{W}_0, 0 \leqslant \overline{\tau} \leqslant 1)$ eventually fall into it, with no exceptions (Fig. 1c). Correspondingly, the time duration of all bounces mapped in D cannot overcome a certain value τ_{max}. Both $\overline{W}_0$ and τ_{max} are functions of α and Γ. The velocity $\overline{W}_0$ was approximated [18] through the impact relations (1)–(2) to

$$\overline{W}_0 = \frac{\alpha\Gamma}{1-\alpha}\left(1 + \sqrt{1 + \frac{4}{\pi\Gamma}\frac{1-\alpha}{1+\alpha}}\right); \tag{3}$$

correspondingly,

$$2\tau_{max} = 1 + \overline{W}_0 + \Gamma + \sqrt{(\overline{W}_0 + \Gamma)^2 + 2\Gamma/\pi}\,. \tag{4}$$

Both approximate laws (3) and (4) improved on earlier estimates [1,4] and compare well with our numerics for relatively large values of A and α;

(iii) *Bouncing trajectories*: The trajectories of a BB can be classified into three categories as shown in Fig. 1:

(a) Chattering trajectories. For most initial conditions the BB gets eventually locked onto the plate through a sequence of infinitely many bounces that take place within a finite phase interval of an ultimate plate oscillation. This class of trajectories is the main concern of the present report;

(b) Periodic trajectories. By definition, the repeating bounce sequence of a periodic trajectory is represented by q points in the $(\overline{\tau}, W)$ space satisfying the periodic conditions $\overline{\tau}_q = \overline{\tau}_0 + k$, $W_q = W_0$. In the simplest case of identical bounces, $q = 1$, the coordinates of the $q = 1$ representative point $(\overline{\tau}_1^{\pm}(k), W_1(k))$ satisfying the above periodic conditions are

$$\left(\frac{1}{2} \pm \frac{1}{2\pi}\arccos\left[\frac{k}{\Gamma}\frac{1-\alpha}{1+\alpha}\right], \frac{2\alpha k}{1+\alpha}\right). \tag{5}$$

Here the periodic trajectories marked by $(-)$ are clearly unstable [8]. The distance of such points from the $\overline{\tau}$-axis increases with the time between bounces k, $k \leqslant \Gamma(1+\alpha)/(1-\alpha)$. Moreover, as shown in Figs. 1c and 4 all these points fall within D and, equivalently, in dimensionless units $k \leqslant \tau_{max}$;

(c) Chaotic trajectories. For a special value of Γ (i.e., of the plate oscillation amplitude) it may happen that a new periodic $q = 1$ solution with period k enters D, namely, $W_k = \overline{W}_0$; for this special value of k, $\overline{\tau}_1^{\pm}(k) = 1/2$ and the $(\pm)$ trajectories coincide. On increasing Γ, only the $(+)$ trajectory is stable, as $\overline{\tau}_1^{\pm}(k)$ shift, respectively, to the right $(+)$ and to the left $(-)$. Note that the relative impact velocity $W_1(k)$ does not depend on Γ, only $\overline{W}_0$ does (it increases with Γ). At even larger Γ values, the k periodic trajectory, too, becomes unstable; a new stable periodic trajectory with $q = 2$ close representative points can be identified instead

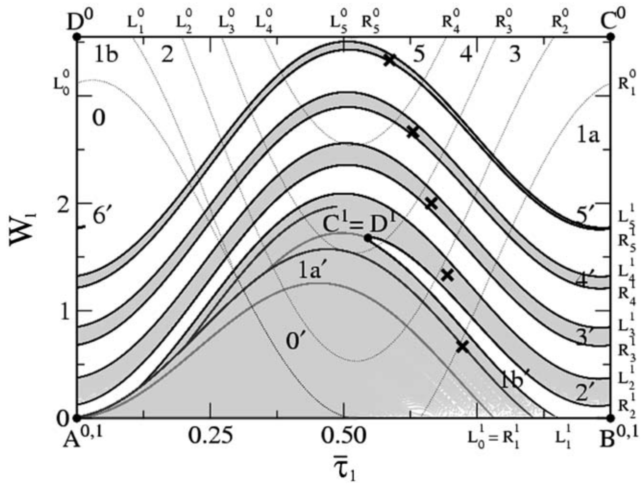

Fig. 4. Mapping rule $D^0 \to D^1$ for $\Gamma = 1.947$ and $\alpha = 0.5$. The frame $(ABCD)^0$ represents D^0. The forward image of the uniform grid sampling D^0, see Fig. 2, is reported for reader's convenience. The curves of the contour $(ABCD)^1$ are also drawn in different gray shades as in Fig. 2. Domains of D^0 and D^1 related through the impact map (1)–(2) carry the same label (primed for D^1). The *stable* periodic trajectories with $q = 1$ and $k = 1$–5 are marked by crosses—one per band with identical label k'.

(*period doubling*). On further increasing Γ this mechanism repeats itself until a persistent chaotic $q = \infty$ trajectory is established, whose representative points populate a twisted curve in D, showing the typical features of a *strange attractor* [4,8]. A numerical analysis of this class of trajectories is reviewed in Section 4.

3. The chattering mechanism

We focus now on the chattering mechanism: this is a process of inelastic collapse that affects all the BB trajectories originated within the trapping region, with the exception of the periodic orbits (a countable set) and of the trajectories also belonging to the basin of attraction of the strange attractors of Section 4.

In view of our definition of the trapping region, we restrict our study of the BB dynamics to the region of initial impact conditions $D^0 \equiv D(\overline{\tau}_0, W_0)$ and determine its forward image D^1 in the $(\overline{\tau}_1, W_1)$ space. In the generic case of Fig. 2, the forward images $(ABCD)^1$ of the boundary lines of D^0, $(ABCD)^0$, are drawn in different gray shades and oriented counterclockwise. In Fig. 2b, the upper D^0 boundary line $(CD)^0$—the black segment $W_0 = \overline{W}_0$—is mapped into an *extended band* structure obtained by wrapping the stretched (τ_1, W_1) image of Fig. 2a around the half-cylinder $(\overline{\tau}_1, W_1)$. The number of extended bands coincides with the maximum time between bounces τ_{max} expressed in units of the plate oscillation period, i.e., the integer part of τ_{max} in dimensionless units. This is apparent in the extended impact representation of Fig. 2a. The image of the $\bar{\tau}_0$-axis (dark gray) is a broken line: the segments $(0, \tau_g)$ and $(1 - \tau_f, 1)$ are mapped into themselves, while the launching segment [1] $(\tau_g, 1 - \tau_f)$ is mapped into a bell-shaped curve plus a dangling arch contained in band 2′. The oriented segment $(BC)^0$ (light gray) is also mapped into a broken line: a bell-shaped curve encircled by the forward image of the $\bar{\tau}_0$-axis and a disconnected arch with end points on the forward image of the $\bar{\tau}_0$-axis and at the branching point $C^1 = D^1$ of the lowest extended bands 1b′ and 2′.

In order to clarify the trapping mechanism, in Fig. 3 we plotted the backward iterate of D^0, D^{-1}, using the gray shade code and the orientation rule earlier adopted in Fig. 2. At variance with D^1, here the pre-image of the $(BC)^0$ segment bisects all (five) extended bands, which branch off above the $(CD)^0$ segment, namely, outside the trapping region D^0.

On combining the contents of Figs. 2 and 3, one determines the mapping rule $D^0 \rightarrow D^1$ illustrated graphically in Fig. 4. The rectangle $(ABCD)^0$ in the impact space containing D^0 and D^1 can be divided up uniquely in special domains related by the implicit map (1)–(2). Indeed, each band of D^1 must be regarded as the map of a uniquely connected D^0 domain, whose boundaries always comprise a portion of the D^0 upper boundary line $W_0 = \overline{W}_0$. Moreover, all the extended bands 2′–6′ intersect the vertical axes $\bar{\tau}_1 = \bar{\tau}_0 = 0$ and $\bar{\tau}_1 = \bar{\tau}_0 = 1$; therefore, the corresponding domains 2–6 of D^0 must be encircled by the backward image of the W_0-axis (Fig. 3b). Analogously, the central area of D^1 corresponds to the domain of D^0 encircled by the pre-image of the $\bar{\tau}_0$-axis and split in two domains, 0 and 1a, by the W_0-axis. The intercepts of the backward iterate of the W_0- and $\bar{\tau}_0$-axis with the D^0 boundaries are labelled L_k^0 and R_k^0 with k running from 0 to 5; their forward image is denoted by L_k^1 and R_k^1, respectively.

3.1. Extended bands

A simple analysis of the impact map (1)–(2) leads to the conclusion that the extrema $(\tilde{\tau}_k, \tilde{W}_k)$ of the continuous arches $\widehat{L_k^0 R_k^0}$ of Fig. 4 satisfy the identity

$$\tilde{W}_k = 2|\tilde{\tau}_k|[1 - \pi\gamma \sin(2\pi|\tilde{\tau}_k|)] , \tag{6}$$

in extended impact notation. As a consequence, their minima shift left, from $\bar{\tau}_k = \tau_g$ to $\bar{\tau}_k = 1/2$, with increasing the index k and separate vertically with unit spacing. In view of the mapping rule illustrated above, the forward image of the segment cutting D^0 vertically at $\bar{\tau} = \tau_g$ bisects to a good approximation all the extended bands of D^1.

Studying the BB dynamics requires computing the forward image of D^0 after n impacts with n arbitrary large. The structure of D^n can be analyzed qualitatively as follows. In Fig. 4, the first iterate D^1 is entirely contained in D^0 and, therefore, divided up among D^0 domains 0–6; the intersections of D^1 with one such domain get mapped inside the D^1 domain carrying the same label; hence D^2 is contained in D^1, see Fig. 5, its volume shrinking as an effect of the impact inelasticity [9]. In conclusion D^n retains the band structure (and labelling) of D^1 with two significant differences, see in Fig. 6: (1) the width of each extended band narrows down to an

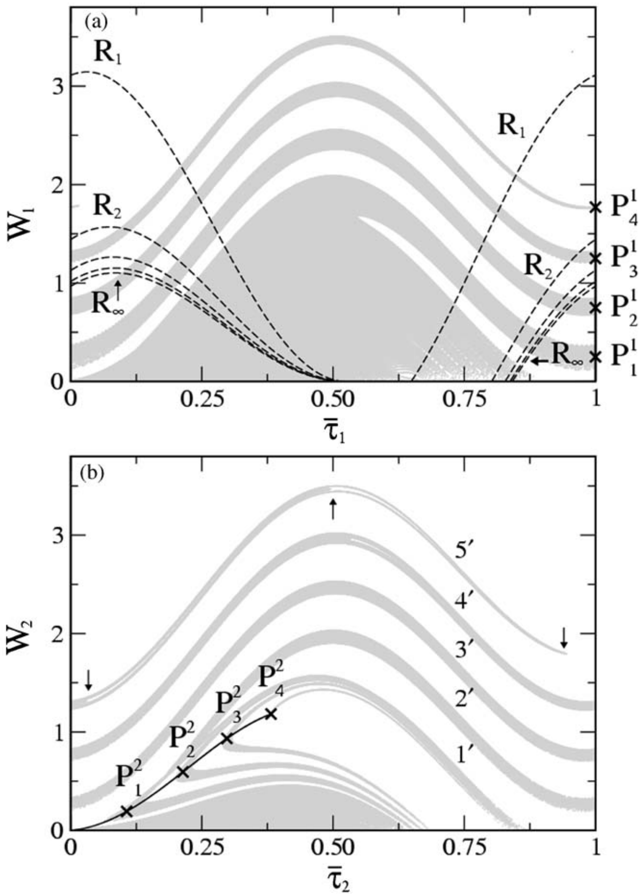

Fig. 5. First, (a), and second, (b), forward iterate of D^0. Dashed curves: backward images R_n of the launching segment $(\tau_g, 1-\tau_f)$; crosses: midpoints P_n^1 of the D^1 extended bands in (a) and their images P_n^2 in (b); thick curves: the W_1 segment $(1, P_4^1)$ in (a) and its image in (b). The vertical arrows in (b) point to the tip of the three sub-bands of band 5′ of D^2.

asymptotic value, while its fine structure gets more and more complicated with increasing n; (2) the domain $0' \cup 1a' \cup 1b'$ of D^1 is replaced by $n-1$ new looped *chattering bands*.

The intricacies of the extended band sub-structure of Fig. 6 can be explained by iterating the mapping rule of Fig. 4. The tip of band 6′ belongs to the domain 0 of D^0; therefore, all its points get mapped into the chattering bands of D^2 contained in domain 0′ - no band 6′ is detectable in Fig. 5 for D^2.

As another example, we notice that domain 5 in Fig. 4 intersects bands 3′–5′ of D^1. The forward image of such three disconnected domains of D^1 consists of three disconnected looped sub-bands embedded in band 5′ of D^2 and intersecting the

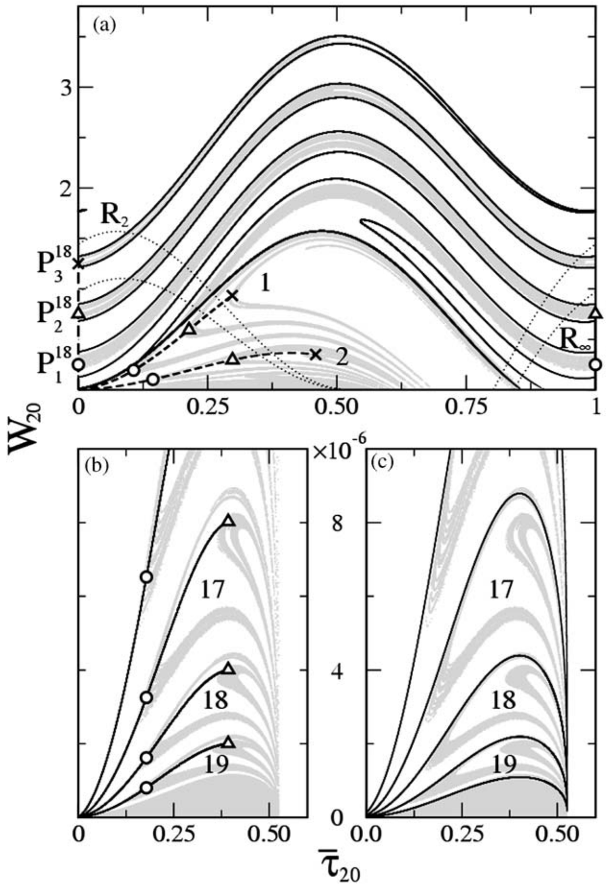

Fig. 6. Chattering band structure of D^{20} plotted against the contour of D^1, with chattering bands labelled 1–19: (a) The midpoints of the three bottom-extended bands after 18 iterations, $P^{18}_{1,2,3}$, and the corresponding first and second forward images (circles, triangles and crosses). The first two forward images of $P^{18}_{1,2,3}$ sit on top of the three sub-bands of the chattering bands 1 and 2, both contained in the chattering region under the bell-shaped thicker black curve; (b) forward image of the midpoints of the two bottom-extended bands of D^1, $P^0_{1,2}$, chosen as initial conditions, after $k = 16$–19 iterations (circles and triangles). In panel (c) the chattering bands displayed in (b) are plotted against the arches of the $k = 16$–20 iterate of the $\bar{\tau}_0$ segment contained by the curve R_∞.

W_0-axis at $\bar{\tau}_0 = 0$; the right- and left-most sub-band tips in Fig. 5 correspond to band $5'$ and $3'$ of D^1, respectively.

Finally, the forward images of the intersections between the bisectrix of the topmost D^1 band and the arch $\widehat{L^0_k R^0_k}$ provide a good estimate of the width of the $k+1'$ band of D^n for large n. When repeated over and over again, this construction (Smale's horseshoe [9,18]) generates the complicated Cantor-like band sub-structure displayed in Fig. 6.

3.2. Chattering bands

The structure of the chattering bands can be analyzed in detail by extending the technique illustrated in Fig. 4. The curves R_n, $n = 1, 2, \ldots$, of Fig. 5a represent the nth backward iterate of the launching segment $(\tau_g, 1 - \tau_f)$ on the $\overline{\tau}_0$-axis. Here R_1 coincides with the curve $\widehat{L_0^0 R_1^0}$ of Fig. 4. By definition, R_1 encloses all the initial impact conditions allowing at least one bounce of the BB in the region $0' \cup 1a'$. Analogously, each of the nested curves R_n encloses the initial conditions of the trajectories that execute n or more bounces in the same region; for $n \to \infty$ the curves R_n quickly approach the curve R_∞ that defines the actual *chattering region*. Note that the forward image of the region delimited by R_1, $0' \cup 1a'$, encompasses all chattering bands—see Figs. 5 and 6.

In Fig. 5a we marked (thicker line) the W_1 segment with end points at $\tau = 1$ and at the midpoint P_4^1 of band $5'$; it contains all midpoints P_{k-1}^1 of each D^1 band k intersecting the W_1-axis. In Fig. 5b the image of such a segment is shown to bisect quite closely the chattering bands of D^2.

Moreover, we have computed 19 iterates of the W_0 segment $[1, P_2^0]$ (only the last four are shown in Fig. 6). As it lies entirely below R_∞ (Fig. 6a), its iterates approach the τ-axis; the kth iterate bisects the corresponding chattering band k and the kth iterate of the points $P_{1,2}^1$, $P_{1,2}^k$, fall on top of the two outer sub-bands of the chattering band k (Fig. 6b). Note that in the case of D^k, with $k \geqslant 2$, R_1 and R_2 intersect three extended bands, while R_n with $n \geqslant 3$ intersect two bands only (compare Figs. 5a and b); accordingly, the chattering bands are split into three (the two topmost bands) or two sub-bands (all remaining lower bands), respectively.

To further characterize the chattering band structure, in Fig. 6c we computed the kth iterate of the chattering region under R_∞. By definition each iterate belongs to the intersection of the chattering region being mapped with the central domain $0' \cup 1a'$. The structure of Fig. 6c clearly shows that the tip of the kth chattering band is embedded in the sector delimited by the kth and the $(k+1)$th iterate of the τ_0-axis.

3.3. Chattering trajectories

More insight in the dynamics of the chattering mechanism may be gained by monitoring the time evolution of single trajectories (Fig. 7), as suggested in Ref. [2]. The chattering bands are visited by the trajectories that have entered the impact region encircled by R_1. Moreover, those originated in the chattering region below R_∞ perform a straight sequence of infinitely many bounces with exponentially decaying amplitude. The representative points $(\overline{\tau}_n, W_n)$ of a chattering trajectory approach the $\overline{\tau}$-axis (Fig. 7a) cascading through the chattering bands according to the asymptotic law $W_n = 2(\overline{\tau}_\infty - \overline{\tau}_n)$. Note that the chattering process is completed within a finite time interval [4,13], negligible with respect to the plate oscillation period. Moreover, the chattering bands overlap the chattering region below R_∞ with the phase comprised in the interval $(0, \tau_g)$, namely, only in $0 \cap (0' \cup 1a')$. As all the

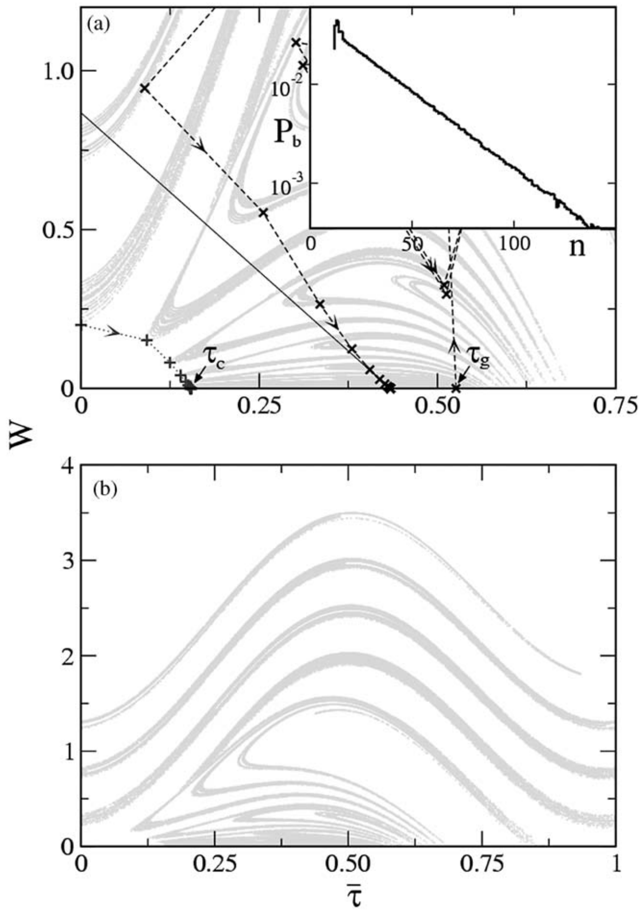

Fig. 7. (a) Chattering trajectories in the impact space $(\overline{\tau}, W)$ as an oriented sequence of impact events represented by $(+)$ for the trajectory initiated at the lower edge of band $3'$ with $\overline{\tau}_0 = 0$, and by $(\times)$ for the BB launched by the platform at $\tau_0 = \tau_g$. The latter trajectory repeats itself after each chattering process. The representative points of D^{20} are reported for the sake of a comparison. Solid line: the fitting law $W_n = 2(\overline{\tau}_\infty - \overline{\tau}_n)$. Inset: Fraction P_b of the trajectories with initial conditions at the grid points of Fig. 4b and entering the layer $0 \leqslant W \leqslant 10^{-6}$ with $\tau_c \leqslant \overline{\tau} \leqslant \tau_g$, after n bounces. The exponential decay of P_b with n is apparent. (b) Noisy trajectory initiated at $\tau_0 = \tau_g$ with $W_0 = 0$. Numerical noise is generated by randomizing the impact parameters as explained in Section 3.3; other simulation parameters are as in panel (a). After 10^6 bounces the trajectory impact points populate both the extended and the chattering bands without undergoing complete chattering.

points of this portion of the impact space are mapped into the lower sides of the chattering bands, so are the chattering trajectories in their final approach to the plate.

The chattering bands clearly accumulate against a finite segment (τ_c, τ_g) of the $\overline{\tau}$-axis *(chattering phase)*. By repeatedly mapping forward the lower edge of band

$3'$ at $\overline{\tau}_0 \simeq 0$, one traces closely the tips of *all* chattering bands and easily evaluates their limiting phase τ_c (Fig. 7a).

The band structure we have illustrated so far is rather robust toward numerical noise. In Fig. 7b we plotted the impact parameters of 10^6 bounces of the re-launching trajectory, where the impact parameters (τ_n, W_n) in (1)–(2) have been modified at each step by adding the small random amounts $\delta\tau$, δW, uniformly distributed in $[-5, 5] \times 10^{-4}$ and $[0, 1] \times 10^{-3}$, respectively. Such a noisy trajectory does not undergo a full chattering process, as the small perturbation we introduced suffices to unlock it from the plate after a finite number of bounces; nevertheless, the topology of the band structure (both extended and chattering) is clearly resolved.

Finally, it should be noticed that chattering resembles inelastic collapse, the process by which partially inelastic balls dissipate their energy through an infinite number of collisions in a finite amount of time [12,13]. In particular, it has been shown that letting the coefficient of restitution approach 1, as the impact velocity goes to 0, makes inelastic collapse disappear [19]. We checked numerically [16] that the BB chattering, too, is suppressed in the limit $\alpha \to 1$ (as signalled by $\overline{W}_0$, Eq. (3), tending to ∞ in the same limit).

4. Searching for strange attractors

Although in Figs. 2–7 we chose BB parameter values such that all D^0 points undergo chattering, the existence of strange attractors in the $(\overline{\tau}, W)$ space (of course, inside the trapping region) is by no means ruled out. Following the indications of Refs. [1–4], in Fig. 8 we lowered the plate acceleration Γ, thus revealing a stable strange attractor in band $5'$. A weak condition of existence (and stability) of such an object can be determined as follows. We know from Section 2.2 that when a $q = 1$ periodic trajectory executes identical bounces with time length k, the maximum value of k compatible with our choice of α and Γ is the integer part of $k_{max} = \Gamma(1 + \alpha)/(1 - \alpha)$. A simple linear stability analysis [1] suggests that bounces of duration k are stable against chattering as long as

$$\sqrt{k_{max}^2 - \frac{4}{\pi^2}\frac{1 + \alpha^2}{1 - \alpha^2}} < k < k_{max} \; . \tag{7}$$

Let us suppose that a new stable periodic trajectory in the topmost extended band k' has appeared for $k = k_{max}(\alpha, \Gamma)$—see also Section 2.2; on increasing Γ, k_{max} grows larger than the *integer* index k denoting the new periodic trajectory, so that both inequalities (7) may hold good and the trajectory keeps being stable; on further increasing Γ the first inequality (7) eventually fails and the kth periodic trajectory becomes unstable. Note that, in view of Eq. (7), the existence of two or more stable trajectories—with decreasing k values—requires α values much closer to one than in our simulation ($\alpha = 0.5$). Furthermore, the smaller k_{max}, the wider the stability domain of the periodic solutions in the (α, Γ) space.

Inequalities (7) clearly define a necessary condition for the existence of a stable chaotic trajectory made of slightly perturbed (i.e., irregular) bounces with time

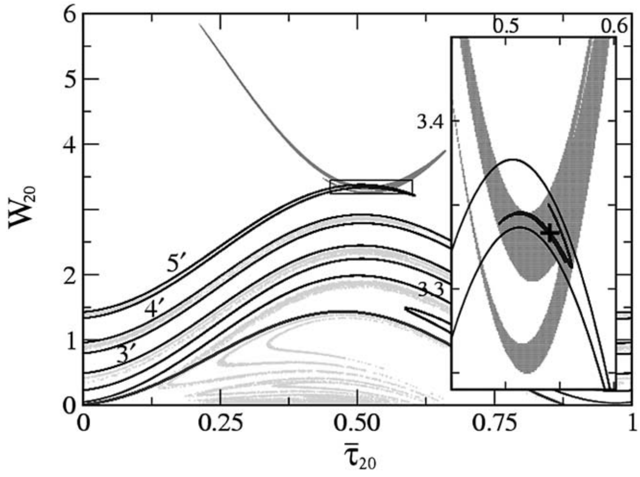

Fig. 8. Strange attractor (dark gray) for $\Gamma = 1.724$, $\alpha = 0.5$ (and $\overline{W}_0 = 3.40$), obtained by recording an individual trajectory for over 10^6 bounces, and corresponding basin of attraction (gray), see text. The relevant band structure of D^{20} (light-gray dots) is plotted against the contour of D^1; the chattering region $0' \cup 1a'$ is delimited by the bell-shaped thicker black curve. The attractor was shown to originate from the periodic trajectory (+) through period doubling; note that both lie well outside D^{20} (see inset), though well inside D^1.

duration close to k, whose representative points diffuse over the strange attractor structures plotted in Figs. 8 and 9.

The presence of a strange attractor does not affect our characterization of the chattering process. All the D^0 trajectories undergoing chattering jump down the ladder formed by the chattering bands. As noticed in Ref. [3], D^n shrinks due the inelasticity ($\alpha < 1$) of the ball-plate collisions, leaving the strange attractor isolated in an emptied portion of the relevant (in most cases, the topmost) extended band of D^1. However, in impact representation it takes a large number n of bounces for the real profile of the strange attractor to emerge, as a "shadow" prolonging it is still apparent in Fig. 9b after $n = 100$ bounces; for much larger n values the points shadowing (i.e., not belonging to) the attractor eventually undergo chattering, thus sparsely populating the lower lying chattering bands. The attractor "shadow" gets depleted over time according to a unique exponential decay law (see inset of Fig. 9b); after 200 bounces the strange attractor has fully emerged; it is populated by about 50% of the initial grid points uniformly sampling D^0.

5. Concluding remarks

We explain now why we made use of the impact representation, as opposed to the stroboscopic representation. The impact representation, sampling a bouncing trajectory at each impact time, allows a detailed analysis of the chattering mechanism; in particular, a chattering BB is sampled infinitely many times within

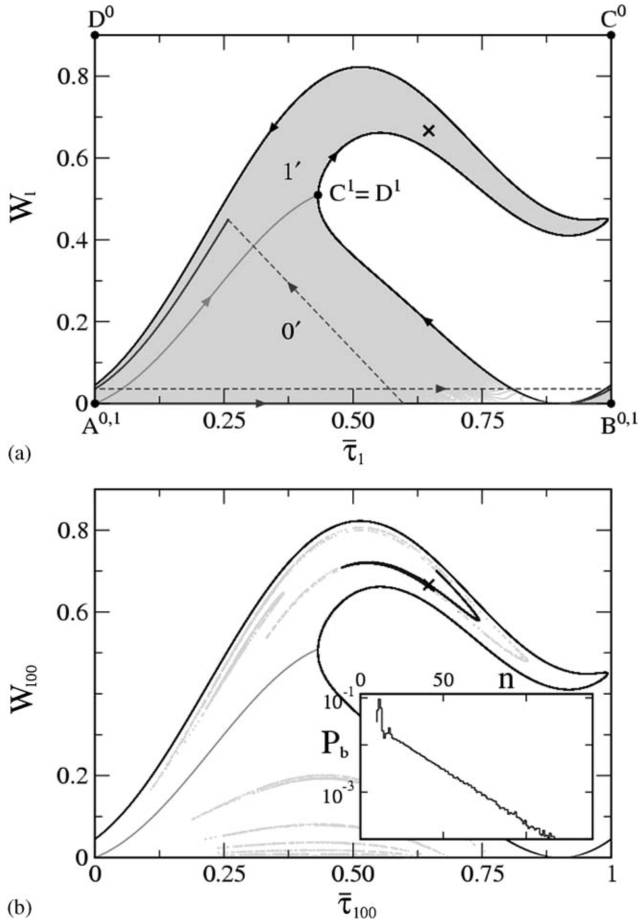

Fig. 9. ''Shadowed'' strange attractor for $\alpha = 0.5$ and $\Gamma = 0.5518$. The strange attractor (dark gray dots), centered around the periodic orbit ($\times$), is obtained by recording an individual trajectory for over 10^6 bounces. In panel (a) the frame is restricted to the countour of D^0; the forward image of each boundary line is plotted in different colors: light gray (W_0-axis), dark gray (τ_0-axis) and black (upper boundary line $\overline{W}_0 = 0.90$). In panel (b) the representative points of D^{100} are reported for the sake of a comparison; the strange attractor continues into a long, looped ''shadow'' formed by points of D^{100} contained in band $1'$. After a large number of bounces (see inset for P_b vs. n; notation as in Fig. 7), the points not belonging to the attractor eventually fall onto the $\overline{\tau}$-axis through a standard chattering mechanism; after 200 bounces the attractor only is distinguishable (i.e., no shadow is visible). The curve AC^1 (light gray) from panel (a) is reported for clarity. Note that the chattering bands are ''open'' (convex arches, not loops) as band $1'$ does not intersect the $\overline{\tau} = 1$ axis.

a fraction of the cycle T. The stroboscopic representation, instead, amounts to a synchronous sampling clocked by the plate oscillations. A high jumping BB with impact parameters $(\overline{\tau}, W)$ in an extended band k' at time nT, gets sampled k times through one complete bounce $nT \to (n+1)T$, namely, it corresponds to a representative point in at least k subsequent stroboscopic images of extended band it belongs to; on the contrary, a BB with impact parameters belonging to the chattering region at nT undergoes full chattering within less than one period T and, therefore, corresponds to no stroboscopic image point at time $(n+1)T$. Thus, the stroboscopic representation tends to filter away chattering versus high jumping trajectories.

A detailed understanding of the BB problem, besides its interest in the theory of dynamical systems, is of potential application to the characterization of the dynamics of a vibrated granular gas. An assembly of identical grains subject to gravity and kept in steady motion through the oscillations of the container bottom (plate) can be modelled by a gas of ideal BBs that collide inelastically with the container walls and the remaining balls [11–13]. For large plate accelerations (i.e., A and/or ω) the grain–grain collisions become less frequent so that the energy loss due to the grain–grain interaction is counterbalanced by the energy injected through the bottom of the container; therefore, one can visualize such a vibrated granular gas as an ensemble of fully randomized BBs to which the stroboscopic analysis may apply with success. Of course, the grain–grain collisions, no matter how low the gas density, are likely to blur the details of the chattering dynamics, ultimately preventing the BB from locking, and to unsettle any chaotic trajectories. Preliminary simulation runs [16] seem to confirm that a characterization of vibrated granular gases along this line is, indeed, viable.

References

[1] J.M. Luck, A. Mehta, Phys. Rev. E 48 (1993) 3988.
[2] A. Mehta, J.M. Luck, Phys. Rev. Lett. 65 (1990) 393.
[3] N.B. Tufillaro, Phys. Rev. E 50 (1994) 4509.
[4] N.B. Tufillaro, T.A. Abbott, J.P. Reilly, An Experimental Approach to Nonlinear Dynamics and Chaos, Addison-Wesley, Reading, MA, 1992.
[5] E. Fermi, Phys. Rev. 75 (1949) 1169.
[6] L.D. Pulstylnikov, Trans. Moscow Math. Soc. 2 (1978) 1.
[7] B.V. Chirikov, Phys. Rep. 52 (1979) 263.
[8] A.J. Lichtenberg, M.A. Lieberman, R.H. Cohen, Physica 1D (1980) 291.
[9] J. Guckenheimer, P. Holmes, Nonlinear Oscillations, Dynamical Systems, and Bifurcation of Vector Fields, Springer, Berlin, 1983 (Chapter 2).
[10] J.M.T. Thompson, H.B. Stewart, Nonlinear Dynamics and Chaos, Wiley, New York, 1991 (Chapter 15).
[11] A. Mehta (Ed.), Granular Matter: An Interdisciplinary Approach, Springer, Berlin, 1994.
[12] H.M. Jaeger, S.R. Nagel, R.P. Behringer, Rev. Mod. Phys. 68 (1996) 1259.
[13] L.P. Kadanoff, Rev. Mod. Phys. 71 (1999) 435.
[14] see e.g. K. Szymanski, Y. Labaye, Phys. Rev. E 59 (1999) 2863;
Z.J. Kowalik, M. Franaszek, P. Pieranski, Phys. Rev. A 37 (1988) 4016.
[15] R. Ramirez, T. Pöschel, N.V. Brilliantov, T. Schwager, Phys. Rev. E 60 (1999) 4465.
[16] S.J. Linz, P. Hänggi, Phys. Rev. E 50 (1994) 3464;
C. Cattuto, F. Marchesoni, F. Nori, (2004) submitted.
[17] P.J. Murphy, D.G. Karr, unpublished.
[18] S. Giusepponi, F. Marchesoni, Europhys. Lett. 64 (2003) 36.
[19] D. Goldman, M.D. Shattuck, C. Bizon, W.D. McCormick, J.B. Swift, H.L. Swinney, Phys. Rev. E 57 (1998) 4831.